Electronic Supplementary Material (ESI) for Analyst.
This journal is © The Royal Society of Chemistry 2020

Supplementary material

ATP induced alteration in peroxidase-like property of hollow Prussian Blue nanocubes: A platform for alkaline phosphatase detection

Jie Lv[a,1], Shuangling Wang[a,1], Cong Zhang[b,*], Yulong Lin[a], Yan Fu[a] and Meng Li[a,*]

[a] *College of Pharmaceutical Sciences, Hebei Medical University, Shijiazhuang, 050017, China.*

[b] *Department of Chemistry, School of Sciences, Hebei University of Science and Technology, Shijiazhuang 050018, China.*

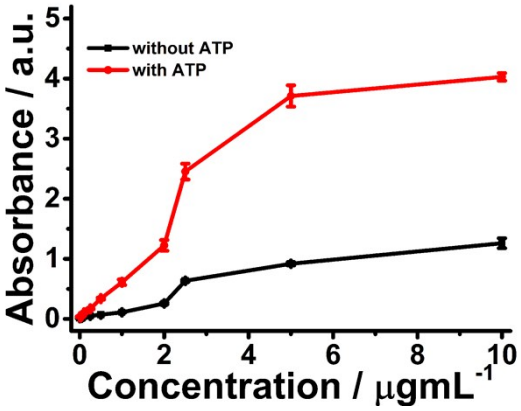

Fig. S1. The absorbance of oxidized TMB in the presence of different concentrations of hPBNCs with or without ATP (10 mM).

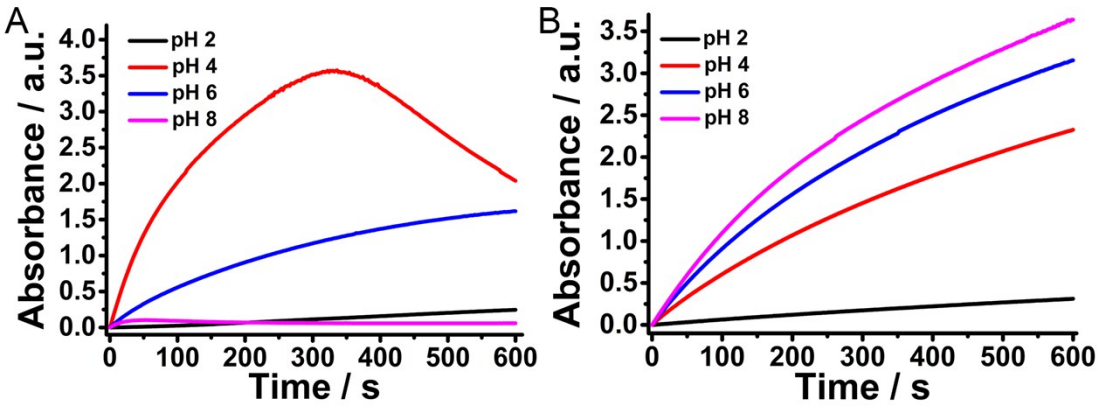

Fig. S2. Time-dependent absorbance changes at 652 nm at different pH values in the absence (A) or presence (B) of 10 mM ATP.

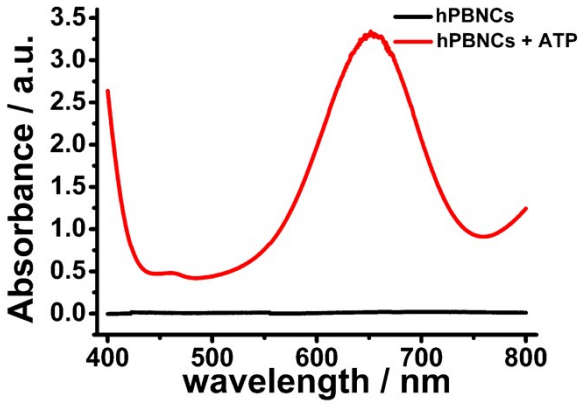

Fig. S3. The catalytic activity of hPBNCs with or without ATP at pH 10.

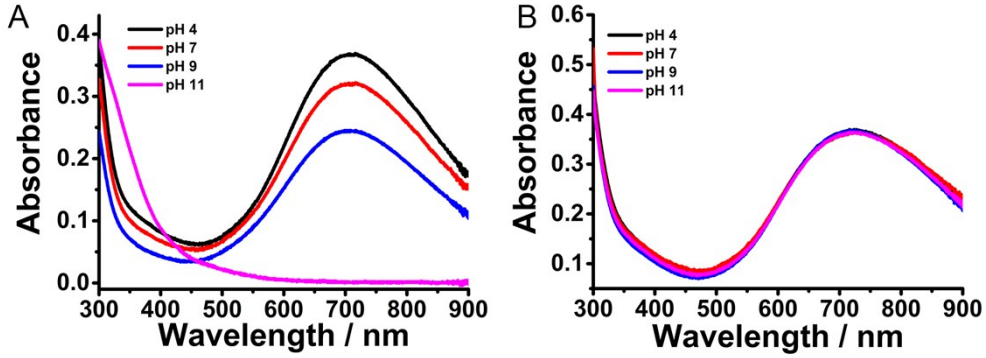

Fig. S4. The UV-vis-NIR absorbance spectrum of hPBNCs in the absence (A) or presence (B) of 10 mM ATP at different pH values.

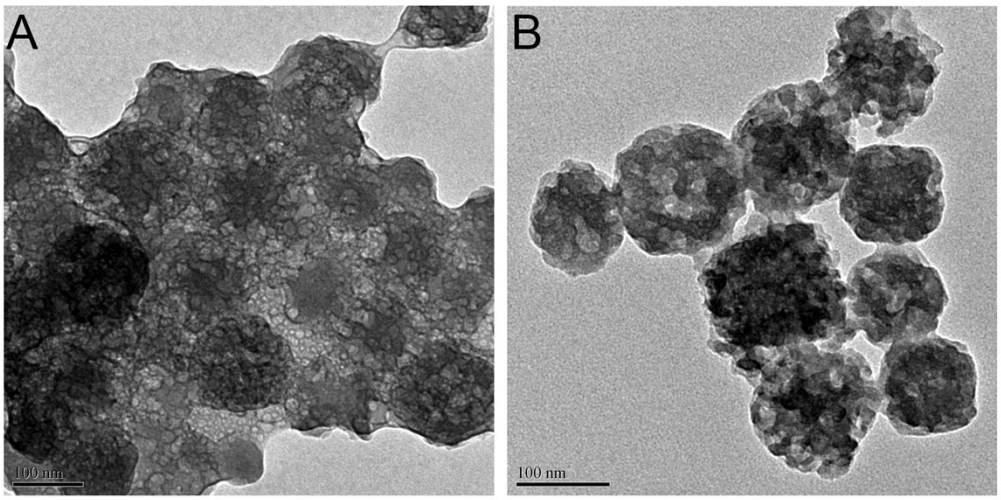

Fig. S5. The TEM images of hPBNCs in the absence (A) or presence (B) of 10 mM ATP at pH 8.

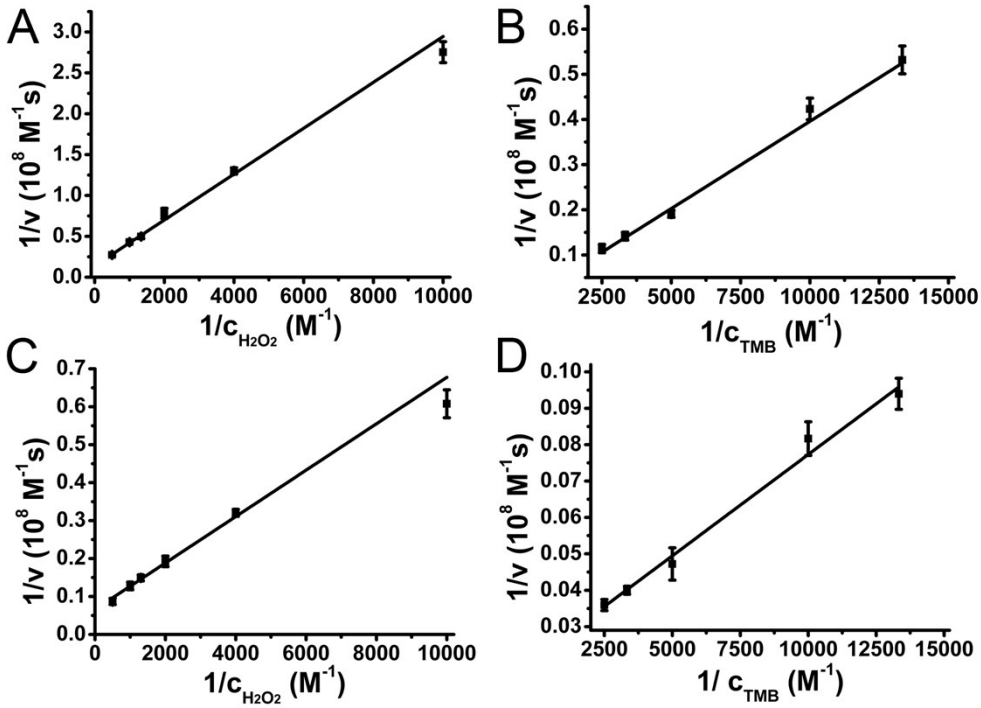

Fig. S6. Steady-state kinetic assay and catalytic mechanism of hPBNCs or hPBNCs-ATP. Lineweaver-Burk plot of the reciprocals of initial rate vs. substrate concentration for the determination of kinetic parameters K_m and V_{max} of hPBNCs (A and B) and hPBNCs-ATP (C and D) with H_2O_2 (left) or TMB (right) as the substrate. Error bars were estimated from three independent measurements.

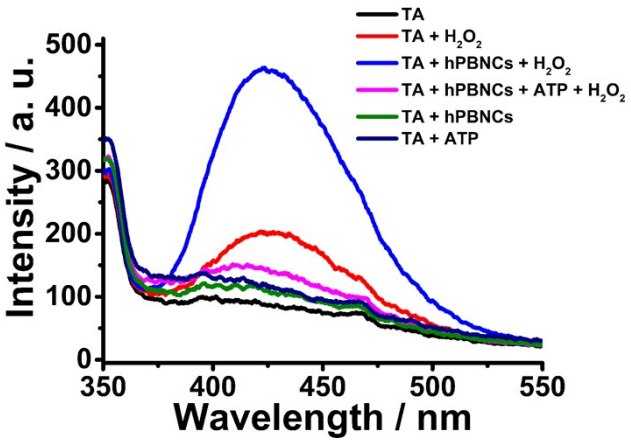

Fig. S7. The formation of •OH radical monitored by TA assay under different conditions.

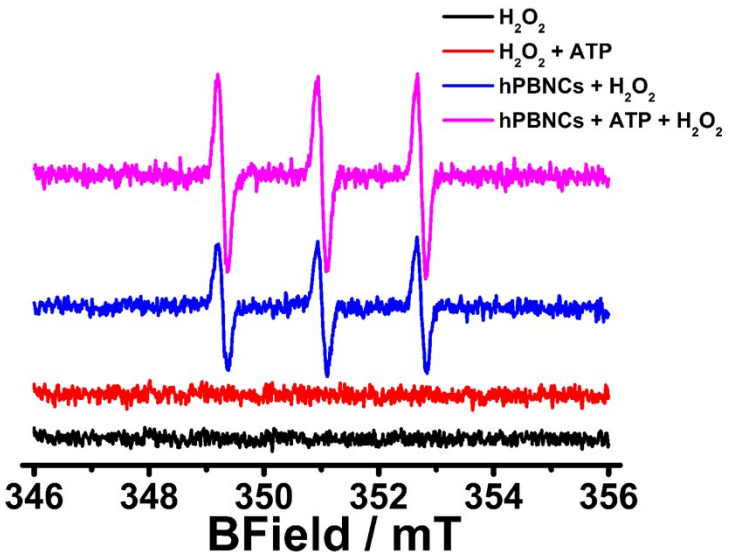

Fig. S8. Characterization of $^1O_2$ signal using ESR spectral method.

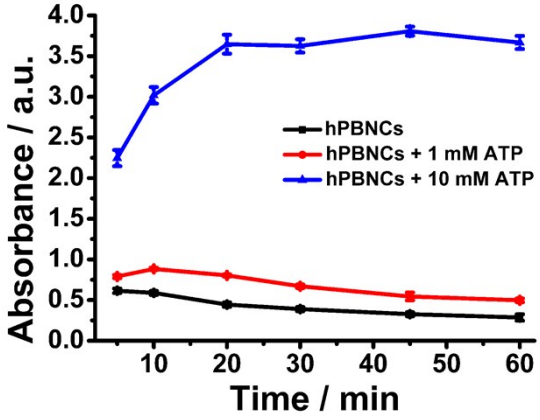

Fig. S9. Time-dependent absorbance changes at 652 nm as a result of the catalyzed oxidation of TMB by hPBNCs with or without different concentrations of ATP.

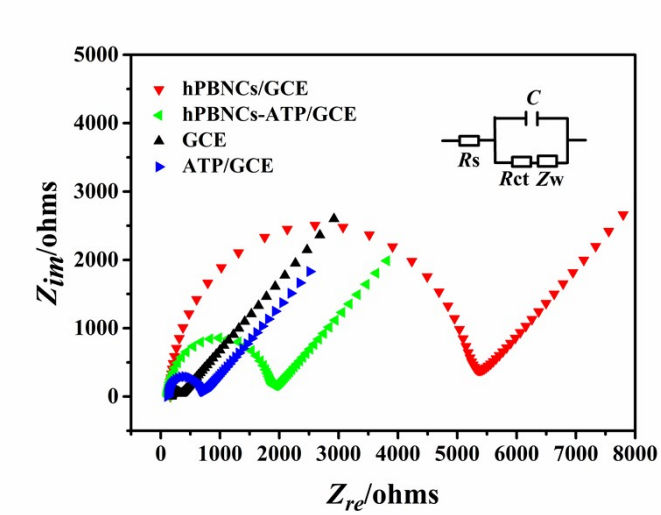

Fig. S10. EIS of GCE, ATP/GCE, hPBNCs/GCE and hPBNCs-ATP/GCE in 0.1 M KCl solution containing 5.0 mM $[Fe(CN)_6]^{-3/-4}$ solution. The frequency range was from 1×10^{-2} to 1×10^{5} Hz. Electrochemical experiments were performed on electrochemical workstation (CHI660D, Shanghai, China) with a conventional three electrode system with the modified electrode as the working electrode, a platinum wire (1 mm diameter) as the counter electrode and an Ag/AgCl electrode (saturated with KCl) as the reference electrode.

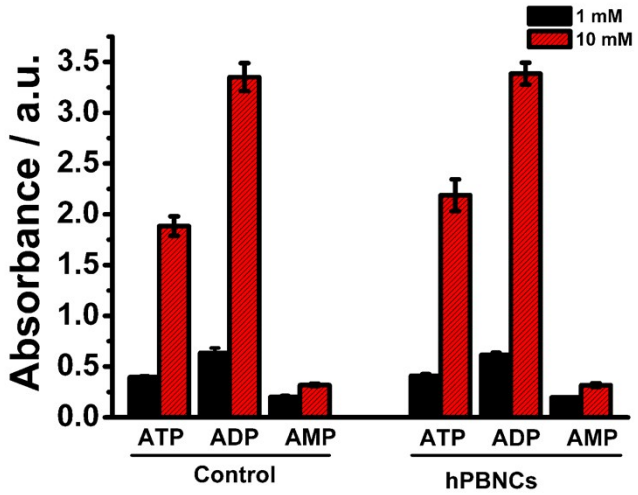

Fig. S11. The free-phosphate productions from hydrolysis of ATP/ADP/AMP in solutions or catalyzed by hPBNCs.

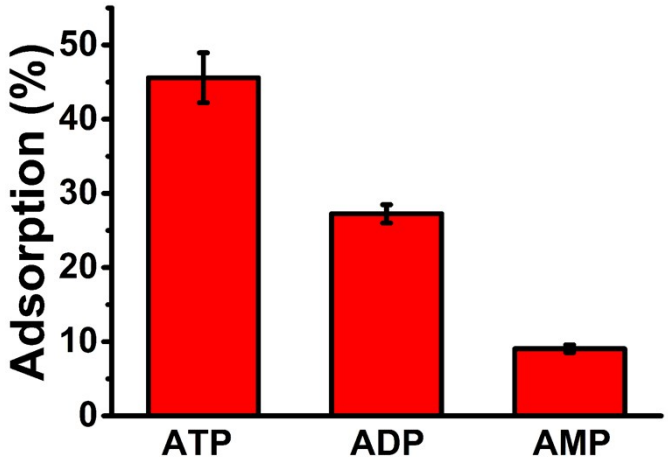

Fig. S12. The adsorption efficiency of ATP, ADP and AMP on hPBNCs. To determine the adsorption efficiency of ATP, ADP and AMP on hPBNCs, ATP/ADP/AMP was incubated with hPBNCs at room temperature for 20 min. After incubation, the mixture was centrifuged and the obtained supernatant was quantified by UV-vis absorption spectroscopy. The absorption efficiency was calculated using the following equation: Adsorption efficiency (%) = $(C_0\text{-}C) / C_0$

where C_0 is the initial concentration of ATP/ADP/AMP, and C is the concentration of the supernatant.

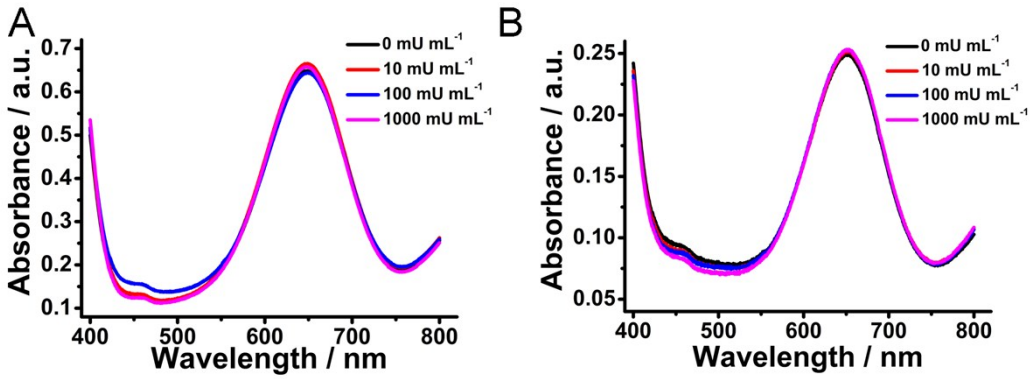

Fig. S13. The effects of ALP with different concentrations on the catalytic activity of hPBNCs at (A) pH 7 and (B) pH 8. The concentration of hPBNCs was 2.5 μg mL^{-1}.

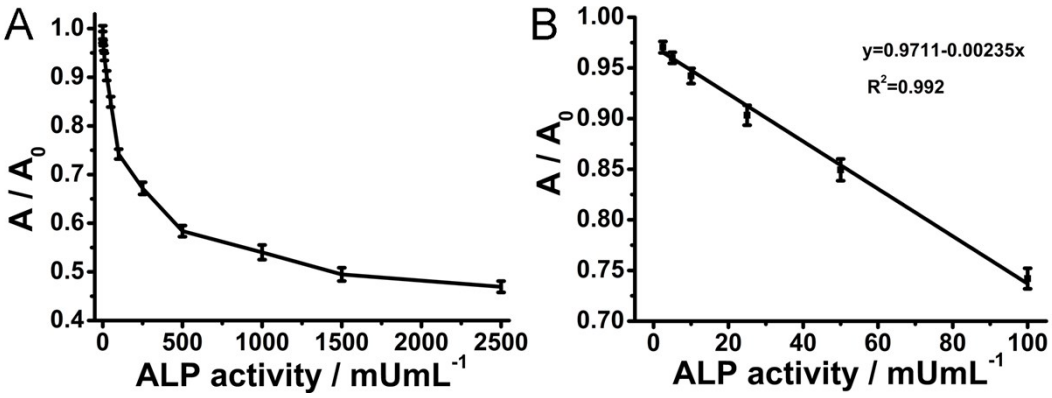

Fig. S14. Detection of ALP activity in mice serum using hPBNCs-ATP system. (A) A dose-response curve for ALP detection using the hPBNCs-ATP system. (B) The linear plots of absorbance measured at 652 nm as a function of the ALP concentration. A_0 and A are the absorbance intensity at 652 nm in the absence and presence of added ALP, respectively.

Table S1. Comparison of recently reported nanozyme-based assay for ALP detection

Nanozyme	LOD	Linear range	Analytic time (min)	References
Copper (II)-based metal-organic frameworks	0.19 mU mL^{-1}	1-34 mU mL^{-1}	90	[1]
MIL-53(Fe)	0.7 mU mL^{-1}	2-80 mU mL^{-1}	110	[2]
Ce-based nanorods	0.1 mU mL^{-1}	0.5-25 mU mL^{-1}	100	[3]
MnO_2 nanosheets	0.05 mU mL^{-1}	0.05-10 mU mL^{-1}	N.A.	[4]
nucleotide coordinated copper ion	0.45 mUmL^{-1}	1-30 mUmL^{-1}	> 120	[5]
G-rich DNA-Cu(II) complex	0.84 mU mL^{-1}	20-200 mUmL^{-1}	80	[6]
hPBNCs	1.54 mU mL^{-1}	2.5-50 mU mL^{-1}	40	This work

References

[1] C. Wang, J. Gao, Y. Cao, H. Tan, Colorimetric logic gate for alkaline phosphatase based on copper (II)-based metal-organic frameworks with peroxidase-like activity, Anal. Chim. Acta. 1004 (2018) 74-81. https://doi.org/10.1016/j.aca.2017.11.078.

[2] K. Ye, L. Wang, H. Song, X. Li, X. Niu, Bifunctional MIL-53(Fe) with pyrophosphate-mediated peroxidase-like activity and oxidation-stimulated fluorescence switching for alkaline phosphatase detection, J. Mater. Chem. B. 7 (2019) 4794-4800. https:// doi.org /10.1039/C9TB00951E.

[3] H. Song, K. Ye, Y. Peng, L. Wang, X. Niu, Facile colorimetric detection of alkaline phosphatase activity based on the target-induced valence state regulation of oxidase-mimicking Ce-based nanorods, J. Mater. Chem. B. 7 (2019) 5834-5841. https:// doi.org /10.1039/C9TB01515A.

[4] F. Tian, J. Zhou, J. Ma, S. Liu, B. Jiao, Y. He, MnO_2 nanosheets as oxidase mimics for colorimetric detection of alkaline phosphatase activity, Microchim. Acta. 186 (2019) 408. https://doi.org/10.1007/s00604-019-3519-1.

[5] H. Huang, J. Bai, J. Li, L. Lei, W. Zhang, S. Yan, Y. Li, Fluorometric and colorimetric analysis of alkaline phosphatase activity based on a nucleotide coordinated copper ion mimicking polyphenol oxidase, J. Mater. Chem. B. 7 (2019) 6508-6514. https://doi.org /10.1039/C9TB01390C.

[6] J. Yang, L. Zheng, Y. Wang, W. Li, J. Zhang, J. Gu, Y. Fu, Guanine-rich DNA-based peroxidase mimetics for colorimetric assays of alkaline phosphatase. Biosens, Bioelectron. 77 (2016) 549-556. https://doi.org/10.1016/j.bios.2015.10.003.